

Vascular biomarkers derived from dynamic contrast-enhanced MRI predict response of vestibular schwannoma to antiangiogenic therapy in type 2 neurofibromatosis

Ka-Loh Li, Ibrahim Djoukadar, Xiaoping Zhu, Sha Zhao, Simon Lloyd, Martin McCabe, Catherine McBain, D. Gareth Evans, and Alan Jackson

Wolfson Molecular Imaging Centre, The University of Manchester, Manchester, UK (K.-L.L., I.D., X.Z., S.Z., A.J.); Institute of Population Health, The University of Manchester, Manchester, UK (K.-L.L., I.D., A.J.); Genomic Medicine, The University of Manchester, Manchester Academic Health Science Centre, Institute of Human Development, Central Manchester NHS Foundation Trust, Manchester Royal Infirmary, Manchester, UK (S.L., D.G.E.); Centre for Paediatric, Adolescent and Young Adult Cancer, Institute of Cancer Sciences, The University of Manchester, UK (M.M.); The Christie NHS Foundation Trust, Manchester, UK (C.M.)

Correspondence Author: Alan Jackson, PhD, FRCR, FRCP, FBIR, Wolfson Molecular Imaging Centre, The University of Manchester, 27 Palatine Road, Manchester, M20 3LJ, UK (alan.jackson@manchester.ac.uk).

Background. Antiangiogenic therapy of vestibular schwannoma (VS) in type 2 neurofibromatosis can produce tumor shrinkage with response rates of 40%–60%. This study examines the predictive value of parameter-derived MRI in this setting.

Methods. Twelve patients with 20 VSs were recruited. Each had at least one rapidly growing tumor. Patients were treated with bevacizumab, 5 mg/kg every 2 weeks. Patients with stable or reduced VS volume were maintained at 2.5–5 mg every 4 weeks after 6 months. Those who failed treatment had their bevacizumab discontinued. Dynamic contrast-enhanced (DCE) MRI performed prior to treatment using a high temporal resolution technique, and data were analyzed to allow measurement of contrast transfer coefficient (K^{trans}), vascular fraction (v_p), extravascular-extracellular fraction (v_e). Relaxation rate (R_{1N}) was measured using a variable flip angle technique. Apparent diffusional coefficient (ADC) was calculated from diffusion-weighted imaging. The predictive power of microvascular parameters and ADC were examined using logistic regression modeling.

Results. Responding tumors were larger ($P < .001$), had lower R_{1N} ($P < .001$), and higher K^{trans} ($P < .05$) and ADC ($P < .01$). They showed increases in R_{1N} ($P < .01$) and reduction of K^{trans} ($P < .01$) and ADC ($P < .01$). Modeling to predict response demonstrated significant independent predictive power for R_{1N} ($B = -0.327$, $P < .001$), and K^{trans} ($B = 0.156$, $P < .05$). Modeling to predict percentage change in tumor volume at 90 days identified baseline tumor volume ($B = 5.503$, $P < .05$), R_{1N} ($B = -5.844$, $P < .05$), and K^{trans} ($B = 5.622$, $P < .05$) as independent significant predictors.

Conclusions. In patients with type 2 neurofibromatosis, biomarkers from DCE-MRI are predictive of VS volume response to inhibition of vascular endothelial growth factor inhibition.

Keywords: bevacizumab, DCE-MRI, neurofibromatosis type 2, prediction, treatment response.

The management of rapidly progressive vestibular schwannoma (VS) is a major clinical problem. This is particularly true in patients with type 2 neurofibromatosis (NF2), in which bilateral VSs are the hallmark of the disease, and multiple other cerebral tumors commonly coexist, complicating treatment planning and limiting surgical options.^{1,2} The benign VS arises

from Schwann cells surrounding the inferior and superior vestibular portion of the eighth cranial nerve.² Progressive tumor growth can cause loss of hearing, and iatrogenic hearing loss can occur following surgical intervention or radiotherapy. As tumors continue to enlarge, they produce increasing brainstem compression that can be fatal. The growth of tumors is highly

Received 5 May 2015; accepted 18 July 2015

© The Author(s) 2015. Published by Oxford University Press on behalf of the Society for Neuro-Oncology. This is an Open Access article distributed under the terms of the Creative Commons Attribution Non-Commercial License (<http://creativecommons.org/licenses/by-nc/4.0/>), which permits non-commercial re-use, distribution, and reproduction in any medium, provided the original work is properly cited.

For commercial re-use, please contact journals.permissions@oup.com.

dependent on the formation of new blood vessels, a process known as angiogenesis. Vascular endothelial growth factor (VEGF) is a ubiquitous proangiogenic cytokine expressed in both sporadic and NF2-related VS. Moreover, the magnitude of VEGF expression has been shown to correlate with tumor growth rate.^{3,4} These observations led to trials of VEGF inhibition strategies, which demonstrated reduction of tumor growth rate, tumor shrinkage,^{5–7} and even tumor regression.^{8,9}

Although the number of such studies remains small, there is clear variation in response rates, which range from 40% to 60%.^{5,6,10} These findings have led others to suggest that antiangiogenic therapy may be appropriate in selected cases of sporadic VS.¹¹ However, as these authors point out, antiangiogenic therapy is extremely costly, which in combination with the slow progression of VS and the variability in growth rates would make clinical trials difficult to conduct. In other tumor types, it was proven possible to predict response to antiangiogenic therapy using biomarkers of the tumor microenvironment derived from dynamic contrast-enhanced magnetic resonance imaging (DCE-MRI)^{12–14} or from diffusion-weighted MRI.¹⁵ In this study we have examined the power of these parameters to predict reduction in the size of VS in patients with NF2 treated with bevacizumab.

Methods

Patient Population

Patients were recruited through the nationally commissioned, highly specialized NF2 clinic in Manchester; UK. All participants gave informed consent, and the National Research Ethics Committee North West approved the study (REC reference 13/NW/0247). Inclusion criteria were: (i) proven NF2 and (ii) at least one VS demonstrating a high growth rate (defined as an increase of 4 mm or greater in the maximal transverse diameter over a 12-month period). In our practice, this growth rate is observed in ~10% of patients with NF2. Exclusion criteria included standard contraindications to MR imaging or contrast-agent administration. Patients were treated with the antivascular endothelial growth factor antibody, bevacizumab, 5 mg/kg every 2 weeks. Where bevacizumab resulted in a reduction in VS volume, treatment at 5 mg/kg every 2 weeks was continued until stability was achieved. Patients in whom there was stability of VS volume were reduced to a maintenance dose of 2.5–5 mg every 4 weeks after 6 months. Those who failed treatment had their bevacizumab discontinued. Clinical response was assessed using a standardized speech discrimination test at 40 dB.

Patients underwent detailed imaging on 2 occasions: pre-treatment (day zero) and 3 months (day 90) following treatment. Follow-up studies with conventional MRI scans were then performed every 3–6 months.

Each VS was classified according to response to antiangiogenic therapy over the 90-day period. Response was defined as a volume reduction exceeding 0.125 cm³ or a relative volume decrease exceeding 5%. These thresholds were defined by a reproducibility study (unpublished results) as the lowest volume change reliably detectable on postcontrast anatomical scans (>95% probability of tumor volume reduction). These criteria differ from standard clinical criteria for volume response since the aim of the work was to identify tumor features that

related to detectable reduction in tumor volume. Progression on treatment was defined as an increase in tumor volume exceeding 0.125 cm³ or a relative volume increase exceeding 5% on the 3- or 6-month follow-up scans.

Magnetic Resonance Imaging

Patients were imaged on a 1.5T whole body scanner (Philips Acheiva, Philips Medical Systems) using an 8-channel head coil. Imaging included anatomical sequences before and after contrast agent administration for measurement of tumor volume. Diffusion-weighted images (DWIs) were collected using 3 B values (0, 400, and 800 s/mm²). DCE-MRI data were collected using a dual-injection technique, as described previously.¹⁶ Contrast agent (CA; gadoterate meglumine; Dotarem, Geubet S.A.) was administered by power injector as an intravenous bolus at a rate of 3 mL/s, followed by a chaser of 20 mL/s of 0.9% saline administered at the same rate. A high temporal resolution (1 s) sequence with a low dose of contrast agent (0.02 mmol/kg) was performed (LDHT-DCE) to allow accurate measurement of the arterial input (AIF) and tissue residue functions. Subsequently, a full CA dose (0.1 mmol/kg), high-spatial resolution (voxel size = 1 × 1 × 2 mm) acquisition (FDHS-DCE) was performed to provide high spatial resolution data and scaling of the AIF. Variable flip angle (VFA; $\alpha = 2^\circ, 8^\circ, 15^\circ$ and 20°) acquisitions were performed prior to the LDHT DCE series for native longitudinal relaxation rate (R_{1N}) mapping.

Image Processing

Analysis of Dynamic Contrast-enhanced MRI

The SI-time curves were converted to contrast concentration curves using measured values of R_{1N} .¹⁷ Using the AIF derived from LDHT-DCE, the LDHT-DCE tissue residue time course curves were fitted to the modified Tofts model.^{18,19} Estimated values of transfer constant (K^{trans}), fractional plasma volume (v_p), and fractional volume of extravascular-extracellular space (v_e) were calculated on a pixel-by-pixel basis. Estimates of bolus arrival time (BAT) were also derived from LDHT-DCE.

Analysis of Diffusion-weighted Imaging

DWI images were used to calculate an apparent diffusion coefficient (ADC). This was done on a pixel-by-pixel basis using inhouse software to fit an exponential decay function to signal intensity. Average values were then derived from the region of interest (ROI).

Co-registration and Tumor Segmentation

Longitudinal co-registration was performed for all scans for each participant. Both 3D-VFA series and images from the LDHT-DCE 4D dynamic series from each visit were co-registered to one precontrast FDHS-DCE 3D dataset acquired on day zero. VSs were segmented using a semiautomatic segmentation program (SX plugin for Osirix, Segmentix, Fr). The results of segmentation were reviewed and, where necessary, edited by an experienced neuroradiologist (A.J.). The resulting 3D ROIs were used to measure tumor volume before and after

treatment and to identify pixels for inclusion in pharmacokinetic analysis (vide supra).

Statistical Analysis

The hypotheses that pretreatment tumor mean values of K^{trans} , v_p , v_e , BAT, $R1_N$, ADC, and tumor volume did not differ between responders and nonresponders was tested using the Mann-Whitney U test. The hypotheses that tumor mean values of K^{trans} , v_p , v_e , BAT, $R1_N$, and ADC in VS were unchanged following treatment was tested using the Wilcoxon signed rank tests.

Binary logistic regression modeling was performed to assess ability of imaging biomarkers to predict tumor response at day 90. The model included tumor volume, $R1_N$ and LDHT-DCE derived measures of K^{trans} , v_p , v_e , BAT, and ADC. All explanatory variables were standardized prior to analysis, and results were expressed as standardized beta coefficients. The predictive performance of the model was assessed by receiver operator characteristics (ROC) analysis and calculation of the area under the curve (AUC). Cross-validation analysis using a leave-one-out methodology was also performed, and classification performance and corresponding cross-validation set was assessed by calculation of sensitivity, specificity, and positive and negative predictive power. Binary logistic regression modeling using the same baseline parameters was also performed to assess the ability of imaging biomarkers to predict progression of the tumor on treatment.

Further linear regression analysis modeling was performed to test the hypothesis that no relationship exists between imaging parameters at baseline and subsequent percentage change in tumor volume. Separate models were performed for each dependent variable using the same explanatory variable datasets described above.

Results

Treatment was well tolerated in all participants with no toxicity greater than grade 1, and in no cases did treatment have to be stopped or withdrawn prematurely. DCE-MRI data were collected in 12 consecutive participants with a total of 20 VSs. Previous surgical resection of a contralateral VS had been performed prior to antiangiogenic treatment in 4 cases. Image quality was high, and no significant movement artefact was apparent in any dataset (Fig. 1). Of these 20 tumors, 12 responded to treatment. These included 2 tumors that had not shown significant growth prior to treatment. There was no response in 8 tumors; 4 of which had shown rapid growth prior to treatment. Imaging biomarker data for all tumors are shown in Table 1. Differences in pretreatment imaging characteristics between responders and nonresponders are shown in Fig. 2. Responding tumors were significantly larger ($P < .001$) and showed lower values of $R1_N$ ($P < .001$) and significantly higher values of K^{trans} ($P < .05$) and ADC ($P < .01$).

Improvements in hearing performance on the word discrimination task were seen in 4 participants, corresponding to significant volumetric tumor response in each case. There was no significant difference in the volume change or percentage volume change in those responding tumors that showed improvement in hearing function and those that did not.

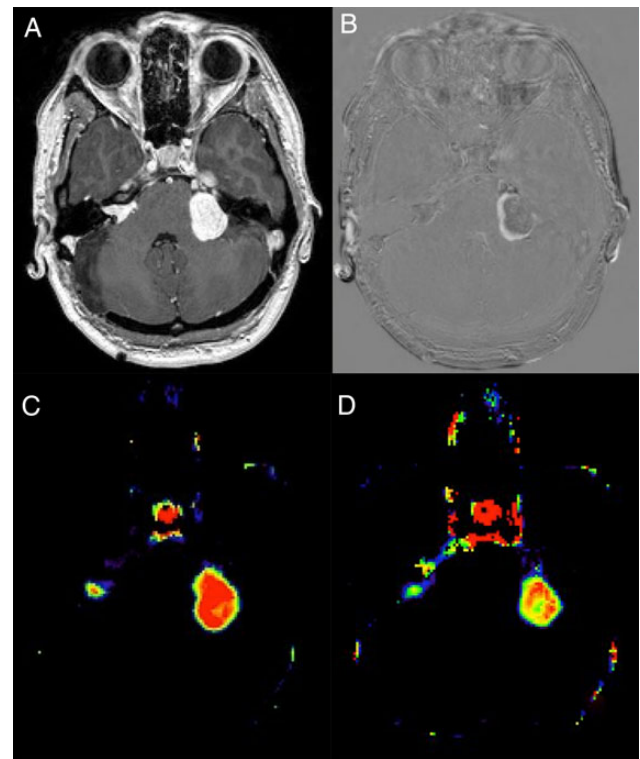


Fig. 1. (A) Contrast-enhanced T1-weighted images of a patient with bilateral vestibular schwannomas. (B) Subtraction image showing volume reduction after 90 days of treatment in the left-sided tumor. (C) K^{trans} image at baseline showing high values in the larger, rapidly growing tumor. (D) K^{trans} image after 90 days of treatment showing marked reduction in the larger tumor.

Table 2 is a correlation matrix showing nonparametric correlation coefficients and significance values for all imaging parameters. Tumor volume correlates with treatment-related volume change ($P < .001$) and percentage volume change ($P < .001$) and correlates inversely with $R1_N$ ($P < .001$). Treatment-related volume change and percentage volume change correlate inversely with $R1_N$ ($P < .001$ and $P < .01$, respectively). Of the pharmacokinetic parameters, K^{trans} correlates with tumor volume ($P < .01$), volume change ($P < .01$), percentage volume change ($P < .05$), and $R1_N$ ($P < .01$), and v_e shows weak correlation with the same parameters ($P < .05$). ADC correlates with tumor volume ($P < .01$), volume change ($P < .01$), percentage volume change ($P < .05$), and K^{trans} ($P < .01$) and correlates inversely with $R1_N$ ($P < .01$).

Following treatment, there was significant reduction in tumor volume ($P < .01$) and increase in $R1_N$ ($P < .05$). Pharmacokinetic parameters from LDHT-DCE showed significant reductions in K^{trans} ($P < .05$) and ADC ($P < .05$). Separate analysis of responding ($n = 12$) and nonresponding ($n = 8$) tumors demonstrated no significant changes in $R1_N$, ADC, or pharmacokinetic parameters in nonresponders. In responders (Fig. 3) there were significant increases in $R1_N$ ($P < .01$) and reduction in ADC ($P < .01$) and K^{trans} ($P < .01$).

Modeling results are summarized in Table 3. Binomial multivariate regression modeling to predict tumor response at 90 days showed $R1_N$ and K^{trans} as the only independent significant predictors of response (Table 1). The area under the ROC curve

Table 1. Data from individual participants with measured tumor volumes at baseline, day 90 and day 180

Patient Number	Sex/ Age*	Tumor Location	R1 _N		K ^{trans**}		ADC**		Tumor Volume			Response, 90 d	Response, 180 d
			0 d	90 d	0 d	90 d	0 d	90 d	0 d	90 d	180 d		
1	M/16	R	0.6223	0.7554	0.1538	0.0666	1238.0	1169.25	10.520	7.382	6.852	res	res
		L	0.6935	0.7402	0.1604	0.0627	1259.8	1115.1	4.389	3.542	3.530	res	res
2	F/25	R	0.6204	0.6705	0.1396	0.1138	1103.6	1133.4	17.870	13.110	12.400	res	res
		L	0.8630	0.9903	0.0879	0.1064	980.4	911.5	0.852	0.993	1.063	non	non
3	M/21	R	0.7123	0.8304	0.0915	0.1116	1123.6	1098.0	1.354	1.236	1.437	non	non
		L	0.8382	0.7762	0.0712	0.0575	825.7	835.9	0.482	0.490	0.509	non	non
4	F/23	R	0.6183	0.6959	0.1325	0.0861	1366.6	1317.2	5.736	4.148	3.705	res	res
		L	0.9430	1.0324	0.0394	0.0450	914.2	718.2	0.407	0.448	0.562	non	non
5	F/16	R	0.6649	0.6909	0.0923	0.0845	1156.4	1131.6	5.932	5.471	5.691	res	res
		L	0.7810	0.8416	0.1127	0.1105	1157.8	892.1	1.096	1.171	NA***	non	NA***
6	M/23	R	0.6338	0.6464	0.1443	0.0798	1354.2	1249.8	4.613	4.077	4.697	res	non
		L	0.7572	0.6777	0.0711	0.0324	854.1	991.8	0.563	0.398	0.612	res	non
7	F/29	R	0.6877	0.6918	0.0989	0.0813	1300.1	1159.1	3.445	3.260	3.173	res	res
		L	1.1578	1.1350	0.1185	0.1142	791.1	558.2	0.196	0.209	0.218	non	non
8	M/20	R	0.6908	0.7157	0.0994	0.1175	1206.2	1217.0	2.962	2.526	NA***	res	NA***
		L	0.6326	0.6830	0.1142	0.0953	1358.2	1490.9	6.406	5.169	NA***	res	NA***
9	F/54	R	0.6137	0.6602	0.1135	0.0739	1248.0	1217.4	8.481	6.288	6.044	res	res
		L	0.6939	0.7680	0.0886	0.0736	1032.8	1179.2	2.067	1.702	NA***	res	NA***
10	M/29	R	0.6939	0.7680	0.0886	0.0736	1032.8	1179.2	2.067	1.702	NA***	res	NA***
		L	0.8984	0.8570	0.0586	0.0635	906.6	907.1	1.147	1.143	1.052	non	non
11	M/26	R	0.9159	0.8575	0.0499	0.0567	987.1	831.0	1.073	1.073	1.085	non	non
		L											

Abbreviations: ADC, apparent diffusion coefficient; L, left; non, nonresponder; R, right; res, responder.

Measured values of R1_N (s⁻¹), K^{trans} (min⁻¹) and ADC (mm²/s) are shown before and following 90 days of treatment.

*Age at baseline MRI scans.

**K^{trans} values are in min⁻¹; ADC values are in 10⁻¹² m²/sec.

***No MRI scans performed at that time.

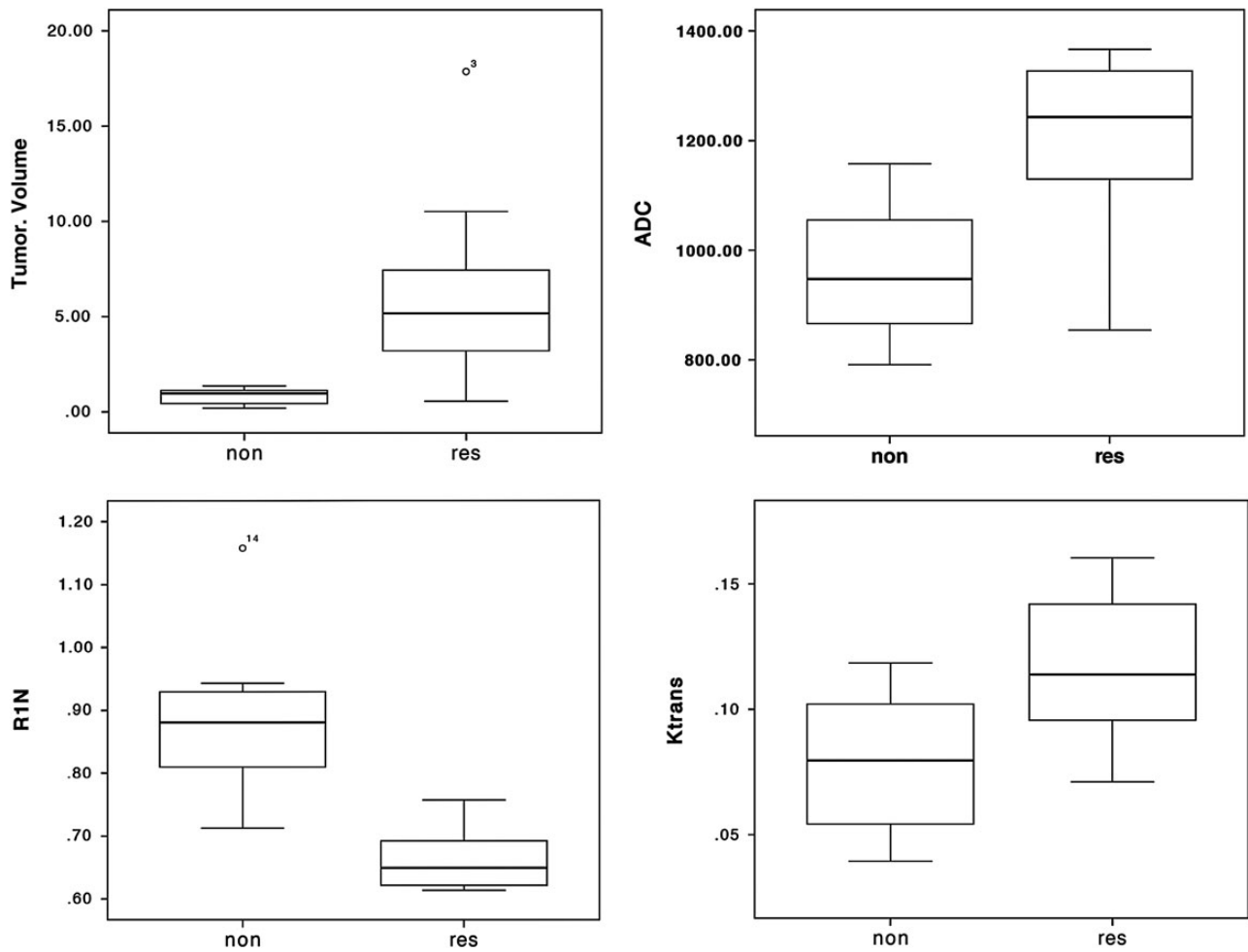


Fig. 2. Comparison of tumor volume (cm³), apparent diffusion coefficient (ADC; mm²/s), (Contrast transfer coefficient; K^{trans} (min⁻¹), and R1_N (longitudinal relaxation; s⁻¹) between responders (res) and ‘nonresponders’ (non). High values of ADC and K^{trans} and low values of R1_N are in keeping with a larger extravascular-extracellular space and increased levels of interstitial free fluid.

Table 2. Correlations between tumor volumetric parameters, dynamic contrast-enhanced MRI-derived parameters, and apparent diffusion coefficient

	Tumor Volume (V)	Change in V	Percentage Change V	R1 _N	K^{trans}	v_p	v_e	ADC
Tumor volume (V)		0.920***	0.711***	-0.932***	0.669**	NS	0.513*	0.758**
Change in V				-0.913***	0.684**	NS	0.562*	-0.662**
Percentage change V				-0.779**	0.562*	NS	0.481*	-0.486*
R1 _N					-0.666**	NS	-0.511*	-0.788***
Ktrans						NS	NS	0.654**
v_p							NS site	NS
v_e								0.504*

Abbreviations: ADC, apparent diffuse coefficient; v_p , plasma volume; NS, not significant; v_e , extravascular extracellular space fraction. Figures represent the Spearman correlation coefficient.

* $P < .05$, ** $P < .01$, *** $P < .001$.

was 0.9896, and results of the cross-validation analysis are shown in Table 2. Linear multivariate regression modeling to predict percentage change in tumor volume response at 90 days

showed significant independent predictive power for baseline tumor volume (standardized beta coefficient = 5.503, $P < .05$) and R1_N (standardized beta coefficient = - 5.844, $P < .01$).

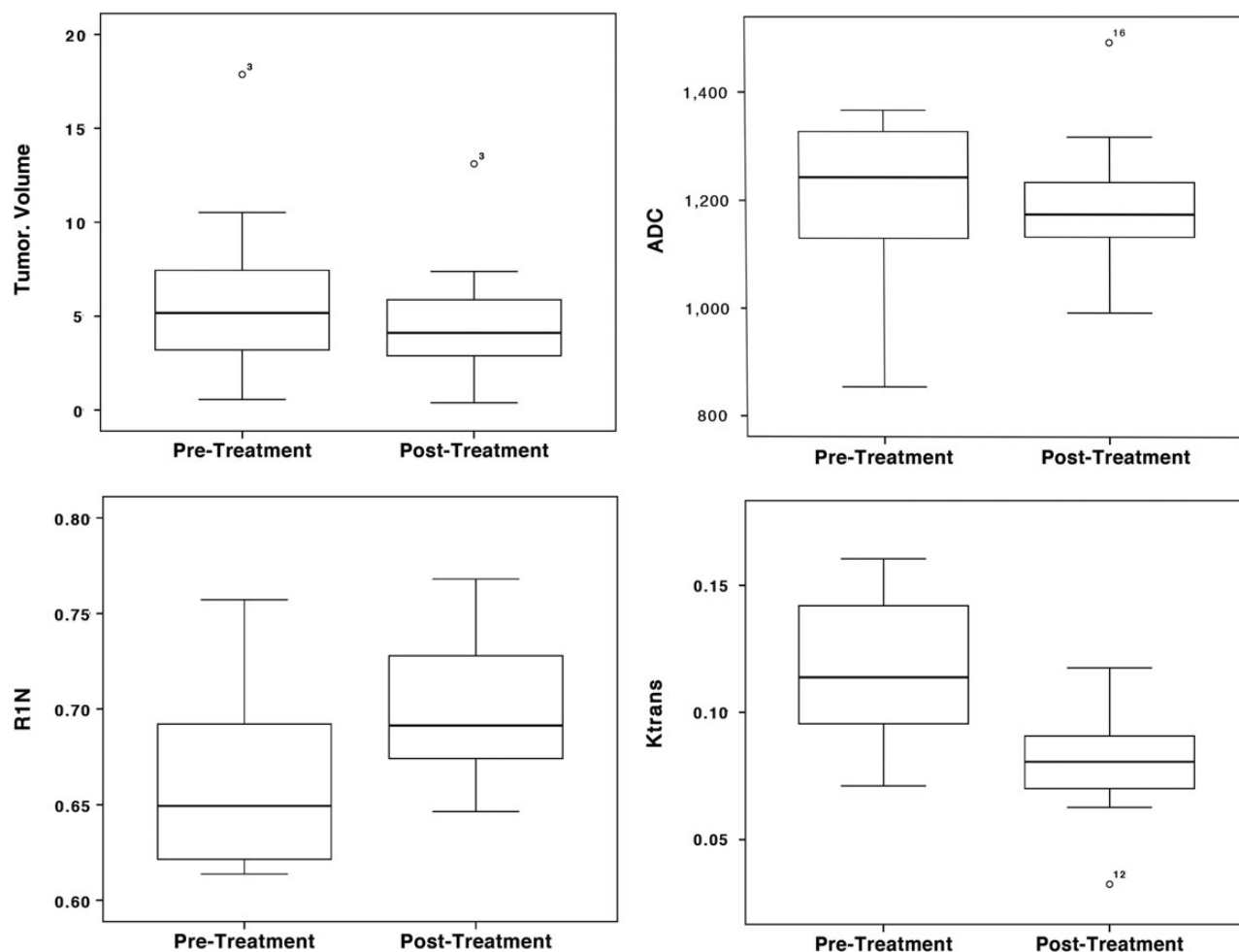


Fig. 3. Changes in tumor volume (cm³), apparent diffusion coefficient (ADC; mm²/s), (Contrast transfer coefficient; K^{trans} (min⁻¹) and R1_N (longitudinal relaxation; s⁻¹) between responders (res) and ‘nonresponders’ (non). Reductions in ADC and increased values of R1_N are in keeping with a decrease in the extravascular-extracellular space and decreased levels of interstitial free fluid.

Table 3. Independent significant variables in binomial linear regression to predict response (top) and multiple linear regression to predict percentage tumor volume change (bottom)

Explanatory Variable	Standardized β Coefficient	Std. Error	T Stat	Significance
Model 1: Prediction of response				
R1 _N (s ⁻¹)	-0.327	0.083	-4.186	$P < .001$
K^{trans} (min ⁻¹)	0.156	0.083	1.902	$P < .05$
Constant	0.6	0.66	9.057	$P < .001$
Model 2: Prediction of percentage volume change				
Tumor Volume (cm ³)	5.503	2.396	2.297	$P < .05$
R1 _N (s ⁻¹)	-5.844	2.357	-2.479	$P < .01$
Constant	10.122	1.727	5.862	$P < .001$

Regression analyses were performed using standardized values.

Calculated AUC, sensitivity and specificity for the original data and for the cross-validated (leave-one-out) dataset for the prediction of response are shown in Table 4.

Progression on treatment was identified in 6 tumors. All 6 had been growing rapidly at presentation, 5 had shown initial response, and one did not. Binomial multivariate regression modeling did not identify any significant predictive features for the identification of tumors that progressed.

Discussion

This study has confirmed the findings of previous researchers, demonstrating shrinkage of VS in 60%, associated with hearing improvement in 33% of cases following treatment with VEGF inhibition. This is similar to the response rate cited by Plotkin et al.⁵ who found a hearing response in 57% and radiographic evidence of tumor shrinkage in 55% over the same time period. A later study reported lower response rates in a series of 12 patients with a radiological response in 39% and associated objective and subjective improvement of neurological symptoms in 60%.¹⁰ Previous studies have adopted the original response criteria suggested by Plotkin of a reduction of $\geq 20\%$ in tumor volume. In addition they examined the duration of

Table 4. Area under the receiver operator curve, sensitivity, and specificity of the binomial regression model for the prediction of tumor response in original data (top) and following leave-one-out cross-validation

Prediction of Response	AUC-ROC	Sensitivity	Specificity
Data	0.979	92	97
Cross-validated	0.894	83	87

Abbreviation: AUC, area under the curve; -ROC, receiver operator characteristic.

Sensitivity and specificity derived from the data are the best performance that can be expected. Leave-one-out analysis gives an approximation of how the prognostic model would be expected to behave in a larger population.

the volume response and the effect on hearing and other neurological symptoms. In this study we have attempted to identify characteristics of the tumor microenvironment that could identify those tumors likely to show this volumetric response. Consequently, we have chosen a more sensitive index of tumor volume change; defining response as any decrease in tumor volume $>5\%$ (or $>0.125\text{ cm}^3$). It must also be appreciated that we have defined response purely as a volumetric reduction at 90 days and have not performed functional imaging at later time points.

Despite the small number of participants in this study, we have clearly identified phenotypic characteristics of the tumor microvasculature that are associated with subsequent response to VEGF inhibition and carry significant independent predictive power. Response was associated with larger tumor size, lower values of R_{1N} , and high values of K^{trans} at baseline. These 3 parameters showed significant cross correlations, but both R_{1N} and K^{trans} were independently and significantly predictive of tumor response. These findings suggest that baseline DCE-MRI may provide sufficient predictive power to support clinical trials and targeted therapy in this patient group, allowing identification of participants in whom volumetric response is unlikely to occur with a sensitivity of 83%–92% and a specificity of 87%–97%. Attempting to predict the resultant percentage change in tumor volume identified baseline tumor volume in addition to the same 2 predictive parameters as independent significant predictors. The expected accuracy of a predictive model based on these features cannot be assessed on such a small data sample since it will require analysis of the distribution of errors in predicted volume. However, these findings suggest that such a model could be developed with a larger dataset. Following treatment, responding tumors showed increases in R_{1N} and reductions in K^{trans} and ADC in association with volume loss. These parameters provide some insight into the mechanisms associated with tumor shrinkage. The R_{1N} measurement inversely reflects the free water content of tissue, so that increases in the parameter following treatment are likely to reflect reductions in interstitial tumor fluid. This is supported by this and previous studies using diffusion-weighted MRI that have identified high values of ADC in solid VSs, suggesting the presence of high amounts of extracellular water in the tumor matrix.²⁰ Furthermore, Plotkin et al.⁵ found high values of ADC as the only radiological feature at baseline that correlated

with changing tumor volume at 3 months. We have also seen a relationship between baseline ADC and tumor shrinkage. However, ADC was a strong correlate of R_1 , and the inclusion of R_1 in the models excluded ADC as an independent significant predictive feature. The K^{trans} parameter reflects regional capillary blood flow, capillary endothelial permeability, and the surface area of the capillary endothelial membrane. Since a primary action of VEGF inhibitors is a rapid reduction in capillary endothelial membrane permeability, reduction of K^{trans} following treatment is likely to reflect this mechanism. However, the possibility that treatment is associated with significant changes in tumor blood flow would provide an alternate interpretation of these findings and would also be in keeping with the concept of vascular normalization in response to antiangiogenic therapy. Previous authors¹¹ have examined the possible therapeutic mechanisms associated with response to VEGF inhibition and concluded: “A possible explanation for the rapid effect of anti-VEGF therapy in both schwannoma size and hearing may be due to a reduction in permeability of peritumoral blood vessels and associated vasogenic edema.” A later study by Wong et al,²¹ using a murine model, demonstrated a 43% decrease in vascular permeability within 24 hours of treatment as well as a decrease in the surface area of vessels of 33%. It is of considerable importance that Wong et al²¹ found an increase in necrosis rather than apoptosis, suggesting cell death resulting from inadequate vascular supply rather than a direct cytotoxic effect. They also showed that the loss of functional Merlin resulted in downregulation in the semaphorin/neuropilin axis, which normally inhibits VEGF signaling. These authors concluded that anti-VEGF therapy most probably controls tumor growth by re-establishing a natural balance between VEGF and semaphorin 3 signaling resulting in vascular normalization. The findings of the current study are entirely in keeping with a primary mechanism of vascular normalization with reduction in intratumor or edema resulting from reductions in endothelial permeability and/or local blood flow. At a simplistic level, the findings may be interpreted as showing that tumors with a greater angiogenic drive, associated with increased endothelial permeability, local blood flow, and consequently with increased interstitial fluid, are more likely to respond and that they do so by normalization of microvascular parameters that result in reversal of each of these features.

In conclusion we have shown that initial volumetric response to anti-VEGF therapy is more likely in VSs that show high levels of intratumoral edema and high values of K^{trans} , reflecting blood flow and capillary endothelial permeability. Responding tumors show reductions in both of these features that correlate with and predict volumetric tumor response. Subsequent progression of the tumor on treatment was not associated with any microenvironmental predictive feature. These findings support suggestions of previous researchers that the primary mechanism of anti-VEGF therapy occurs through vascular normalization and provide a potential selection criteria for targeted therapy.

Funding

This work was jointly funded by Cancer Research UK (CRUK) and the Engineering and Physical Sciences Research Council (EPSRC). Funding reference C8742/A18097.

Acknowledgments

This work is an output of the CRUK EPSRC Cancer Imaging Center in Cambridge and Manchester.

Conflicts of interest statement. None declared.

References

1. Lloyd SK, Evans DG. Neurofibromatosis type 2 (NF2): diagnosis and management. *Handb Clin Neurol.* 2013;115:957–967.
2. Evans DG, Stivaros SM. Multifocality in neurofibromatosis type 2. *Neuro Oncol.* 2014;17(4):481–482.
3. Caye-Thomasen P, Baandrup L, Jacobsen GK, Thomsen J, Stangerup SE. Immunohistochemical demonstration of vascular endothelial growth factor in vestibular schwannomas correlates to tumor growth rate. *Laryngoscope.* 2003;113(12):2129–2134.
4. Caye-Thomasen P, Werther K, Nalla A, et al. VEGF and VEGF receptor-1 concentration in vestibular schwannoma homogenates correlates to tumor growth rate. *Otol Neurotol.* 2005;26(1):98–101.
5. Plotkin SR, Merker VL, Halpin C, et al. Bevacizumab for progressive vestibular schwannoma in neurofibromatosis type 2: a retrospective review of 31 patients. *Otol Neurotol.* 2012;33(6):1046–1052.
6. Plotkin SR, Stemmer-Rachamimov AO, Barker FG II, et al. Hearing improvement after bevacizumab in patients with neurofibromatosis type 2. *N Engl J Med.* 2009;361(4):358–367.
7. Hawasli AH, Rubin JB, Tran DD, et al. Antiangiogenic agents for nonmalignant brain tumors. *J Neurol Surg B Skull Base.* 2013;74(3):136–141.
8. Mautner VF, Nguyen R, Kutta H, et al. Bevacizumab induces regression of vestibular schwannomas in patients with neurofibromatosis type 2. *Neuro Oncol.* 2010;12(1):14–18.
9. Eminowicz GK, Raman R, Conibear J, Plowman PN. Bevacizumab treatment for vestibular schwannomas in neurofibromatosis type two: report of two cases, including responses after prior gamma knife and vascular endothelial growth factor inhibition therapy. *J Laryngol Otol.* 2012;126(1):79–82.
10. Alanin MC, Klausen C, Caye-Thomasen P, et al. The effect of bevacizumab on vestibular schwannoma tumour size and hearing in patients with neurofibromatosis type 2. *Eur Arch Otorhinolaryngol.* 2014; doi:10.1007/s00405-014-3398-3.
11. London NR, Gurgel RK. The role of vascular endothelial growth factor and vascular stability in diseases of the ear. *Laryngoscope.* 2014;124(8):E340–E346.
12. Flaherty KT, Rosen MA, Heitjan DF, et al. Pilot study of DCE-MRI to predict progression-free survival with sorafenib therapy in renal cell carcinoma. *Cancer Biol Ther.* 2008;7(4):496–501.
13. LaViolette PS, Cohen AD, Prah MA, et al. Vascular change measured with independent component analysis of dynamic susceptibility contrast MRI predicts bevacizumab response in high-grade glioma. *Neuro Oncol.* 2013;15(4):442–450.
14. Akisik MF, Sandrasegaran K, Bu G, Lin C, Hutchins GD, Chiorean EG. Pancreatic cancer: utility of dynamic contrast-enhanced MR imaging in assessment of antiangiogenic therapy. *Radiology.* 2010;256(2):441–449.
15. Pope WB, Qiao XJ, Kim HJ, et al. Apparent diffusion coefficient histogram analysis stratifies progression-free and overall survival in patients with recurrent GBM treated with bevacizumab: a multi-center study. *J Neurooncol.* 2012;108(3):491–498.
16. Li KL, Buonaccorsi G, Thompson G, et al. An improved coverage and spatial resolution—using dual injection dynamic contrast-enhanced (ICE-DICE) MRI: a novel dynamic contrast-enhanced technique for cerebral tumors. *Magn Reson Med.* 2012;68(2):452–462.
17. Zhu XP, Li KL, Kamaly-Asl ID, et al. Quantification of endothelial permeability, leakage space, and blood volume in brain tumors using combined T1 and T2* contrast-enhanced dynamic MR imaging. *J Magn Reson Imaging.* 2000;11(6):575–585.
18. Tofts PS. Modeling tracer kinetics in dynamic Gd-DTPA MR imaging. *J Magn Reson Imaging.* 1997;7(1):91–101.
19. Fritz-Hansen T, Rostrup E, Sondergaard L, Ring PB, Amtrup O, Larsson HB. Capillary transfer constant of Gd-DTPA in the myocardium at rest and during vasodilation assessed by MRI. *Magn Reson Med.* 1998;40(6):922–929.
20. Sener RN. Diffusion magnetic resonance imaging of solid vestibular schwannomas. *J Comput Assist Tomogr.* 2003;27(2):249–252.
21. Wong HK, Lahdenranta J, Kamoun WS, et al. Anti-vascular endothelial growth factor therapies as a novel therapeutic approach to treating neurofibromatosis-related tumors. *Cancer Res.* 2010;70(9):3483–3493.